

## Elastic Softening of Surface Acoustic Wave Caused by Vacancy Orbital in Silicon Wafer

Keisuke Mitsumoto<sup>1</sup>, Mitsuhiro Akatsu<sup>1</sup>, Shotaro Baba<sup>1</sup>, Rie Takasu<sup>1</sup>, Yuichi Nemoto<sup>1</sup>, Terutaka Goto<sup>1\*</sup>, Hiroshi Yamada-Kaneta<sup>2</sup>, Yuji Furumura<sup>3</sup>, Hiroyuki Saito<sup>4</sup>, Kazuhiko Kashima<sup>4</sup>, and Yoshihiko Saito<sup>5</sup>

<sup>1</sup>Graduate School of Science and Technology, Niigata University, Niigata 950-2181, Japan

<sup>2</sup>Department of Electrical Engineering and Electronics, Kyushu Institute of Technology, Kitakyushu 804-8550, Japan

<sup>3</sup>Philtech Inc., Bunkyo, Tokyo 113-0033, Japan

<sup>4</sup>GlobalWafers Japan Co., Ltd., Seiro, Niigata 957-0197, Japan

<sup>5</sup>Toshiba Corporation, Yokohama 225-8522, Japan

(Received September 13, 2013; accepted December 6, 2013; published online February 7, 2014)

We have performed surface acoustic wave (SAW) measurements to examine vacancies in a surface layer of a boron-doped silicon wafer currently used in semiconductor industry. A SAW with a frequency of  $f_s = 517$  MHz was optimally generated by an interdigital transducer with a comb gap of  $w = 2.5$   $\mu\text{m}$  on a piezoelectric ZnO film deposited on the (001) silicon surface. The SAW propagating along the [100] axis with a velocity of  $v_s = 4.967$  km/s is in agreement with the Rayleigh wave, which shows an ellipsoidal trajectory motion in the displacement components  $u_x$  and  $u_z$  within a penetration depth of  $\lambda_p = 3.5$   $\mu\text{m}$ . The elastic constant  $C_s$  of the SAW revealed the softening of  $\Delta C_s/C_s = 1.9 \times 10^{-4}$  below 2 K down to 23 mK. Applied magnetic fields of up to 2 T completely suppress the softening. The quadrupole susceptibilities based on the coupling between the electric quadrupoles  $O_u$ ,  $O_v$ , and  $O_{zx}$  of the vacancy orbital consisting of  $\Gamma_8$ – $\Gamma_7$  states and the symmetry strains  $\varepsilon_u$ ,  $\varepsilon_v$ , and  $\varepsilon_{zx}$  associated with the SAW account for the softening and its field dependence on  $C_s$ . We deduced a low vacancy concentration  $N = 3.1 \times 10^{12}/\text{cm}^3$  in the surface layer within  $\lambda_p = 3.5$   $\mu\text{m}$  of the silicon wafer. This result promises an innovative technology for vacancy evaluation in the fabrication of high-density semiconductor devices in industry.

### 1. Introduction

Acoustic waves propagating on a free surface of substrate matter were investigated for the first time by Rayleigh.<sup>1)</sup> One hundred years later, electronic technology has widely adopted a surface acoustic wave (SAW) in miniature electronic modules of ladder-type delay lines, resonators, and band-pass filters using an interdigital transducer (IDT) with high-Q resonance and low insertion loss.<sup>2–5)</sup> The SAW is regarded as a diagnostic tool for investigating  $4f$ -electronic states of rare-earth compounds,<sup>6–8)</sup> quantized Hall effects,<sup>9,10)</sup> topological insulators,<sup>11)</sup> and graphene.<sup>12)</sup> The observation of vacancies in the surface layer of substrate silicon wafers currently used in semiconductor industry is a prominent issue in the diagnostic application of the SAW.

Silicon wafers contain two different types of intrinsic point defects, which consist of a vacancy denoting an unoccupied lattice site and a silicon interstitial corresponding to a silicon atom at an irregular lattice site. The low-temperature softening of the elastic constants of boron-doped silicon observed by bulk ultrasonic waves was successfully described in terms of the quadrupole susceptibilities of a vacancy orbital with a  $\Gamma_8$  quartet ground state and a  $\Gamma_7$  doublet excited state at 1 K.<sup>13–16)</sup> Since the fabrication of semiconductor devices for information technology is carried out using the active region beneath the surface of the substrate silicon wafer, the evaluation of vacancy concentration in the surface layer of the silicon wafer is keenly required. No research on vacancy evaluation in the surface layer of silicon wafers has been reported so far to the best of our knowledge.

In the present study, we show low-temperature measurements of the elastic constant of the SAW propagating on a boron-doped silicon wafer. The excitation of the SAW using an IDT and low-temperature SAW measurement are described in Sect. 2. The low-temperature elastic softening of the

SAW and its magnetic field dependence are presented in Sect. 3. The equations of motion for specifying the SAW on the silicon surface and the quadrupole susceptibilities for the vacancy orbital for describing the softening are shown in Sect. 4. We give our discussion in Sect. 5 and our conclusions in Sect. 6.

### 2. Experimental Procedure

We fabricated an IDT on a boron-doped silicon wafer of  $\#9018$ , which was sliced from a Czochralski (CZ) silicon ingot with a diameter of 300 mm. The wafer shows a resistivity range of 21–23  $\Omega\text{-cm}$  at room temperature indicating a boron concentration of about  $0.7 \times 10^{15}/\text{cm}^3$ . An infrared spectrometer detected an absorption peak at  $1107\text{ cm}^{-1}$  of interstitial atomic oxygen with a concentration of  $1.0 \times 10^{18}/\text{cm}^3$  in the wafer. Using a laser cutter, we reduce the diameter of the wafer concerned from 300 to 200 mm. Because we placed an order for the optimized treatment of 200 mm wafers with inland semiconductor facilities, all steps for the IDT fabrication for the SAW measurement are needed to process the wafers with the same diameter of 200 mm.

A piezoelectric ZnO film was deposited on the (001) surface of the wafer using an AC-sputtering method. The hexagonal  $c$ -axis of the ZnO film is aligned perpendicular to the surface of the wafer. Aluminum (Al) comb-shaped electrodes were fabricated on the ZnO film. There were two cut-in patterns of 5-tooth-comb fingers with a separation gap of  $w = 2.5$   $\mu\text{m}$  and a finger length of 2.025 mm as the design rule  $800w$ . Ordinary semiconductor processing by photoresist lithography and reactive ion etching was used to pattern the IDT.

The sample of  $\#9018$ -8 with a rectangular shape of  $10 \times 20 \times 0.775\text{ mm}^3$  was diced out from the center of the wafer of  $\#9018$ . A schematic view of the IDT is shown in

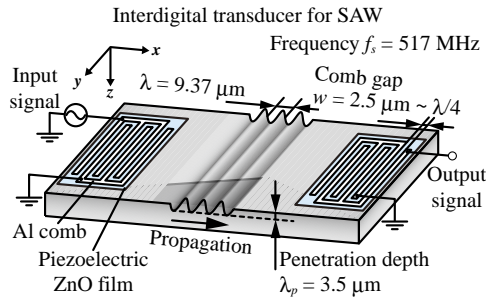


**Fig. 1.** (Color online) Schematic view of the IDT for the SAW measurements on the silicon wafer.

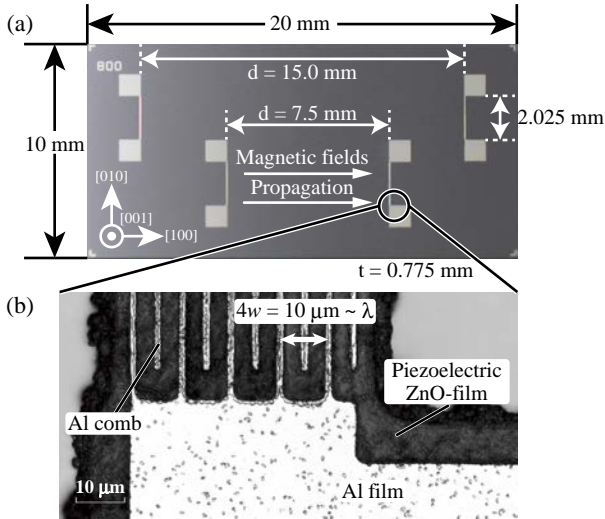


**Fig. 2.** (Color online) (a) Top view of the IDT fabricated on a silicon sample with the (001) surface diced out to  $10 \times 20 \times 0.775 \text{ mm}^3$ . A pair of IDTs with a distance of  $d = 7.5 \text{ mm}$  fabricated on the lower side was employed in the present SAW measurements. The magnetic fields were applied along the [100] axis parallel to the propagation direction of the SAW. (b) Expanded view of the Al comb electrode deposited on the piezoelectric ZnO film photographed by a laser microscope.

Fig. 1. The SAW propagates along the  $x$ -direction on the  $z$  surface of the silicon wafer. The IDT consisting of Al electrodes with a comb gap of  $w = 2.5 \text{ }\mu\text{m}$  fabricated on the piezoelectric ZnO film was designed to optimally generate the SAW with a wavelength of  $\lambda \sim 4w$ . The opposite IDT receives the traveled SAW.

Figure 2(a) shows a top view of the sample on which two pairs of IDTs were placed. One IDT consists of a pair of sender and receiver electrodes. They are separately placed facing each other with distances of  $d = 15.0 \text{ mm}$  in the upper line and  $d = 7.5 \text{ mm}$  in the lower line. The present SAW measurements were carried out on the lower line with  $d = 7.5 \text{ mm}$ . Figure 2(b) shows an expanded view of the Al comb electrode of the IDT photographed by a laser microscope.

The low-temperature elastic softening of the SAW was measured using a dilution refrigerator (Oxford Instruments Kelvinox 400HA), which was equipped with coaxial lines of CuNi tubes for efficient transmission of high-frequency electronic signals of the SAW.<sup>17)</sup> The sample of  $\#9018\text{-}8$  for the SAW measurements was placed in thermal contact with a Ag plate with 1.5 mm in thickness. The Ag plate was attached to a Cu rod of an extended tail from a mixing chamber for

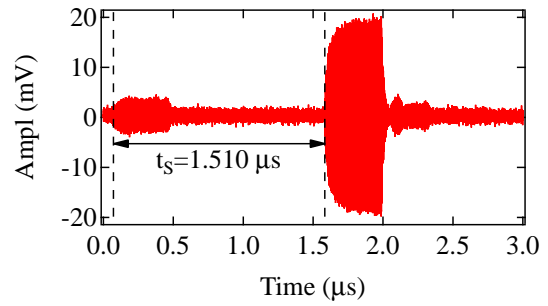


**Fig. 3.** (Color online) Pulsed shape SAW traveled from the sender IDT to the receiver IDT, which is  $d = 7.5 \text{ mm}$  away from the sender, on the (001) surface of the silicon wafer. A time of flight  $t_s = 1.510 \text{ }\mu\text{s}$  gives a group velocity  $v_s = d/t_s = 4.967 \text{ km/s}$  of the SAW.

thermal grounding using a Ag wire with a diameter of 1.0 mm. The adoption of the Ag plate has the advantage of minimizing low-temperature nuclear specific heat enhancement in applying magnetic fields.<sup>18,19)</sup> The temperature of the sample was measured using a calibrated RuO<sub>2</sub> resistance. A superconducting magnet with a bore of 77 mm was equipped to the dilution refrigerator for the generation of magnetic fields of up to 9 T.

The SAW with a pulsed shape of  $0.3 \text{ }\mu\text{s}$  width at a repetition rate of 1 kHz was generated. The velocity change  $\Delta v_s/v_s$  of the SAW as a function of temperature and magnetic field was determined by measuring by phase delay of the pulsed shape SAW. The relatively high frequency of  $f_s = 517 \text{ MHz}$  in the SAW measurements has the advantage of a high resolution better than  $\Delta v_s/v_s = 10^{-6}$ . This excellent resolution leads to the reliable detection of low vacancy concentrations in the silicon wafer.

### 3. Results

The IDT sends an incident pulsed shape SAW of  $0.3 \text{ }\mu\text{s}$  in width with a carrier wave of frequency  $f_s = 517 \text{ MHz}$ . The pulsed shape SAW travels along the [100] direction on the (001) surface to the opposite IDT receiver. As is shown in Fig. 3, a time of flight of  $t_s = 1.510 \text{ }\mu\text{s}$  for the signal received gives a group velocity of  $v_s = d/t_s = 4.967 \text{ km/s}$  at 4.2 K. This corresponds to a wavelength  $\lambda_s = v_s/f_s = 9.61 \text{ }\mu\text{m}$ , which is fairly consistent with the wavelength  $4w = 10 \text{ }\mu\text{m}$  expected from the IDT design. Furthermore, the experimentally determined group velocity  $v_s = 4.967 \text{ km/s}$  of the SAW on the silicon wafer is in agreement with the Rayleigh wave velocity  $v = 4.844 \text{ km/s}$ , which is theoretically calculated using the equations of motion for the SAW in Sect. 4.1. The velocity  $v_s = 4.967 \text{ km/s}$  and density  $\rho = 2.330 \text{ g/cm}^3$  of the silicon wafer give an elastic constant  $C_s = \rho v_s^2 = 5.748 \times 10^{10} \text{ J/m}^3$  for the SAW at low temperatures.

Figure 4 shows the temperature dependence of the elastic constant  $C_s$  of the SAW propagating along the [100] axis on the (001) surface of the silicon wafer. Appreciable softening with a relative change  $\Delta C_s/C_s = 1.9 \times 10^{-4}$  below 2 K down to 23 mK was observed. As is shown in the theoretical expression of Eq. (39) in Sect. 4.2, the amount of softening of  $C_s$  is proportional to the vacancy concentration  $N$  in the surface layer of the silicon wafer. In Fig. 4, we schematically picture the dangling bonds of  $\phi_1, \phi_2, \phi_3,$  and  $\phi_4$  at the vacancy site with a cubic site symmetry of  $T_d$  in the silicon

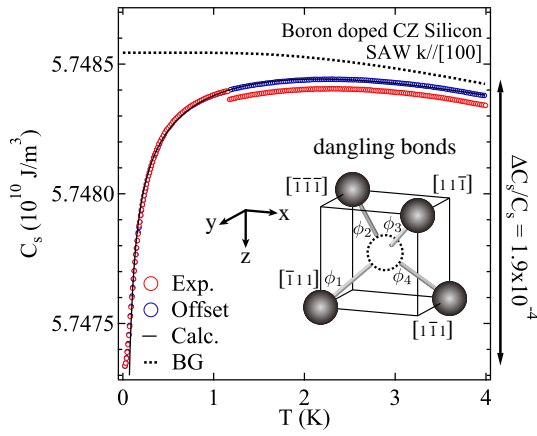


**Fig. 4.** (Color online) Low-temperature softening of the elastic constant  $C_s$  of the boron-doped silicon wafer of  $\#9018-8$ . The SAW propagating along the  $[100]$  direction with the  $(001)$  surface was used for the measurements. The discontinuity at 1.17K is an extrinsic phase shift due to the superconducting transition of the Al comb electrodes used in the IDT. The solid line is a fit in terms of the quadrupole susceptibilities. A schematic view of the four dangling bonds  $\phi_i$  ( $i = 1, 2, 3, 4$ ) of a vacancy is also shown.

lattice, which form the vacancy orbital and bring about the softening of  $C_s$ .

There exists a distinct discontinuity in  $C_s$  at 1.17 K of Fig. 4. This is caused by a superconducting transition of the Al film used in the comb electrodes of the IDT. The slight modification in the effective impedance of the Al comb electrodes brings about an extrinsic phase shift at 1.17K in superposing on the phase delay of the traveled SAW. Nevertheless, the softening of  $C_s$  is properly analyzed by the quadrupole susceptibility of the vacancy orbital in Sect. 4.2 in merely offsetting the extrinsic phase shift at 1.17K. The solid line in Fig. 4 is a fit using a theoretical expression Eq. (39), which is described in terms of the quadrupole susceptibility of Eq. (34) in Sect. 4.2.

In Fig. 5(a), we show the low-temperature dependence of the  $C_s$  of the SAW below 0.8K down to 23 mK at applied magnetic fields of up to 2.0 T along the  $[100]$  axis parallel to the propagation direction. The appreciable softening was observed at zero magnetic field, while the softening was considerably reduced at applied magnetic fields of 0.4 and 1.0 T. The higher magnetic field of 2.0 T fully suppresses the low-temperature softening of  $C_s$ .

The inset of Fig. 5(a) shows the magnetic field dependence of  $C_s$  of the SAW up to 6 T at low temperatures. The appreciable increase in the amount of  $\Delta C_s/C_s = 1.9 \times 10^{-4}$  at a base temperature of 23 mK with increasing magnetic fields from zero to 6 T in the inset of Fig. 5(a) is well consistent with the amount of softening of  $\Delta C_s/C_s = 1.9 \times 10^{-4}$  below 2 K down to 23 mK at zero magnetic field shown in Fig. 4(a). The increased temperature of 0.3 K reduces the field dependence to  $\Delta C_s/C_s = 0.7 \times 10^{-4}$ . Further increase in temperatures to 0.7, 1.5, and 4.0 K completely smears out the field dependence of  $C_s$ . We show the results of the theoretical calculation by the solid and dashed lines in Fig. 5(b). Details of the calculation of  $C_s$  at the magnetic fields in terms of the quadrupole susceptibilities are shown in Sect. 4.2.

Phase shifts associated with the critical field  $H_c \sim 0.02$  T of the superconducting phase in the Al electrodes were

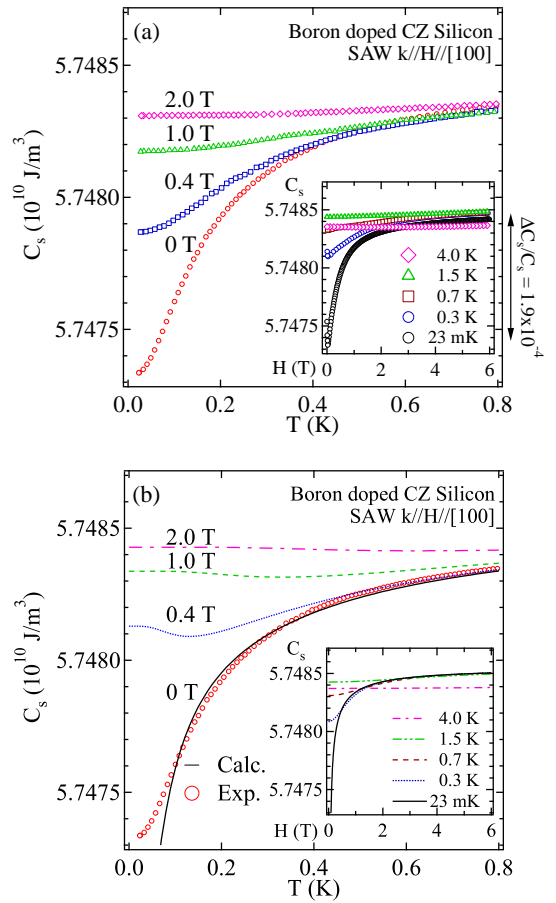


**Fig. 5.** (Color online) (a) Temperature dependence of the elastic constant  $C_s$  of the SAW on the boron-doped silicon wafer of  $\#9018-8$  below 0.8 K down to 23 mK at applied magnetic fields along the  $[100]$  axis. The inset shows the magnetic field dependence of  $C_s$  at low temperatures. Anomalies associated with the superconducting critical field of the Al comb electrodes were observed at 0.02 T. (b) Theoretical calculation of temperature dependence of  $C_s$  in terms of the quadrupole susceptibilities. The inset shows the magnetic field dependence of the calculation of  $C_s$  at low temperatures.

observed in the inset of Fig. 5(a). The alternative adoption of Cu electrodes of a normal metal instead of Al electrodes can be favorable for avoiding the extrinsic phase shift due to the superconducting transition in Al electrodes.

#### 4. Theory

##### 4.1 Equations of motion for SAW

We shall treat equations of motion for the SAW propagating along the  $x$ -direction on the  $z$  surface of the substrate silicon wafer.<sup>20,21</sup> We set a free space for  $z < 0$  and a solid region for  $z > 0$ . This boundary condition gives constraint for stress components of  $\sigma_{iz}$  ( $i = x, y, z$ ) acting on the free  $z$  surface as

$$\begin{aligned} \sigma_{xz} = \sigma_{zx} &= C_{44}\epsilon_{zx} = C_{44}\left(\frac{\partial u_x}{\partial z} + \frac{\partial u_z}{\partial x}\right) = 0, \\ \sigma_{yz} &= C_{44}\epsilon_{yz} = C_{44}\left(\frac{\partial u_z}{\partial y} + \frac{\partial u_y}{\partial z}\right) = 0, \\ \sigma_{zz} &= C_{12}(\epsilon_{xx} + \epsilon_{yy}) + C_{11}\epsilon_{zz} \\ &= C_{12}\left(\frac{\partial u_x}{\partial x} + \frac{\partial u_y}{\partial y}\right) + C_{11}\frac{\partial u_z}{\partial z} = 0. \end{aligned} \tag{1}$$

Here,  $u_i$  ( $i = x, y, z$ ) denote the displacement vector components, and  $C_{11}$ ,  $C_{12}$ , and  $C_{44}$  denote the bulk elastic constants of the silicon lattice with a cubic symmetry. The elastic strains  $\varepsilon_{ij}$  ( $i, j = x, y, z$ ) are defined as<sup>22)</sup>

$$\begin{aligned}\varepsilon_{xx} &= \frac{\partial u_x}{\partial x}, \\ \varepsilon_{yy} &= \frac{\partial u_y}{\partial y}, \\ \varepsilon_{zz} &= \frac{\partial u_z}{\partial z}, \\ \varepsilon_{yz} &= \frac{\partial u_z}{\partial y} + \frac{\partial u_y}{\partial z}, \\ \varepsilon_{zx} &= \frac{\partial u_x}{\partial z} + \frac{\partial u_z}{\partial x}, \\ \varepsilon_{xy} &= \frac{\partial u_y}{\partial x} + \frac{\partial u_x}{\partial y}.\end{aligned}\tag{2}$$

The SAW propagating along the  $x$ -direction on the  $z$  surface leads to a constraint that the displacement vector components  $u_x$  and  $u_z$  are relevant and  $u_y$  is irrelevant. The SAW propagating along the  $x$ -direction keeps the angles for the  $x$ - $y$  and  $y$ - $z$  axes orthogonal. The equations of motion for the SAW consisting of the displacement components  $u_x$  and  $u_z$  in each infinitesimal volume are described as

$$\begin{aligned}\rho \frac{\partial^2 u_x}{\partial t^2} &= C_{11} \frac{\partial^2 u_x}{\partial x^2} + C_{44} \frac{\partial^2 u_x}{\partial z^2} + (C_{12} + C_{44}) \frac{\partial^2 u_z}{\partial z \partial x}, \\ \rho \frac{\partial^2 u_z}{\partial t^2} &= C_{11} \frac{\partial^2 u_z}{\partial z^2} + C_{44} \frac{\partial^2 u_z}{\partial x^2} + (C_{12} + C_{44}) \frac{\partial^2 u_x}{\partial x \partial z}.\end{aligned}\tag{3}$$

The SAW with the displacement components  $u_x$  and  $u_z$  propagates along the  $x$ -axis with a phase velocity  $v$  and a wavenumber  $k = 2\pi f/v$  for a frequency  $f$ . Furthermore, the SAW penetrates into the silicon surface along the  $z$ -axis for  $z > 0$ . Therefore,  $u_x$  and  $u_z$  are given as

$$\begin{aligned}u_x &= \sum_{i=1}^2 U_i \exp[-kq_i z + ik(x - vt)], \\ u_z &= \sum_{i=1}^2 W_i \exp[-kq_i z + ik(x - vt)].\end{aligned}\tag{4}$$

Here,  $\sum_{i=1}^2$  means the sum over two solutions of penetration factors  $q_i$  ( $i = 1, 2$ ) for the  $z$ -axis.  $U_i$  and  $W_i$  denote amplitude of  $u_x$  and  $u_z$  of the SAW, respectively.

Substituting  $u_x$  and  $u_z$  of Eq. (4) into Eq. (3), we obtain simultaneous equations

$$\begin{aligned}(C_{11} - \rho v^2 - C_{44}q_i^2)U_i + (C_{12} + C_{44})q_i(iW_i) &= 0, \\ (C_{12} + C_{44})q_i U_i - (C_{44} - \rho v^2 - C_{11}q_i^2)(iW_i) &= 0.\end{aligned}\tag{5}$$

The second line of Eq. (5) gives a relation between the amplitude of  $U_i$  and  $W_i$  as

$$iW_i = \frac{(C_{12} + C_{44})q_i}{C_{44} - \rho v^2 - C_{11}q_i^2} U_i = \gamma_i U_i.\tag{6}$$

Here,  $\gamma_i$  is a ratio denoting the difference in the amplitude and phase between  $U_i$  and  $W_i$ :

$$\gamma_i = \frac{(C_{12} + C_{44})q_i}{C_{44} - \rho v^2 - C_{11}q_i^2}.\tag{7}$$

Nontrivial solutions of Eq. (5) require an equation for the determinant:

$$\begin{vmatrix} C_{11} - \rho v^2 - C_{44}q_i^2 & (C_{12} + C_{44})q_i \\ (C_{12} + C_{44})q_i & -C_{44} + \rho v^2 + C_{11}q_i^2 \end{vmatrix} = 0.\tag{8}$$

Equation (8) gives an algebraic equation of  $q_i$  as

$$C_{11}C_{44}q_i^4 - \{C_{11}(C_{11} - \rho v^2) + C_{44}(C_{44} - \rho v^2) - (C_{12} + C_{44})^2\}q_i^2 + (C_{11} - \rho v^2)(C_{44} - \rho v^2) = 0.\tag{9}$$

Now we shall go back to the boundary conditions of the stress tensor  $\sigma_{iz} = 0$  acting on the free  $z$  surface at  $z = 0$  of Eq. (1). Substituting Eq. (4) into Eq. (1), we obtain simultaneous equations for  $U_1$  and  $U_2$  as

$$\begin{aligned}U_1(\gamma_1 - q_1) \exp[-kq_1 z] \\ + U_2(\gamma_2 - q_2) \exp[-kq_2 z] &= 0, \\ U_1(C_{12} + C_{11}\gamma_1 q_1) \exp[-kq_1 z] \\ + U_2(C_{12} + C_{11}\gamma_2 q_2) \exp[-kq_2 z] &= 0.\end{aligned}\tag{10}$$

Nontrivial solutions of Eq. (10) require that the determinant should satisfy

$$\begin{vmatrix} \gamma_1 - q_1 & \gamma_2 - q_2 \\ C_{12} + C_{11}\gamma_1 q_1 & C_{12} + C_{11}\gamma_2 q_2 \end{vmatrix} = 0.\tag{11}$$

Using the  $\gamma_i$  of Eq. (7) and the  $q_i$  of Eq. (9), we obtain an algebraic equation from the determinant of Eq. (11):

$$\left(1 - \frac{C_{11}}{C_{44}}R\right) \left(1 - \frac{C_{12}^2}{C_{11}^2} - R\right)^2 = R^2(1 - R).\tag{12}$$

Here, we introduce the ratio of the elastic constant  $C_s = \rho v^2$  of the SAW to the bulk elastic constant  $C_{11}$  as  $R = C_s/C_{11}$ .

Substituting the elastic constants  $C_{11} = 15.681$ ,  $C_{12} = 6.181$ , and  $C_{44} = 8.063$  in  $10^{10}$  J/m<sup>3</sup> units at 4.2 K<sup>15)</sup> and the mass density  $\rho = 2.330$  g/cm<sup>3</sup> of the silicon into Eq. (12), we obtain three solutions for SAW velocities of  $v = 4.844$ , 8.341, and 11.873 in km/s units. Among them, the lowest velocity of  $v = 4.844$  km/s corresponds to the Rayleigh wave, while other higher velocities signify the pseudo SAW.<sup>23)</sup> The group velocity  $v_s = 4.967$  km/s determined by the time of flight of the pulsed shape SAW in Fig. 3 is in fair agreement with the lowest velocity  $v = 4.844$  km/s of the Rayleigh wave in the calculation of Eq. (12).

Substituting the solution  $v = 4.844$  km/s and the bulk elastic constants of the silicon crystal into Eq. (9), we obtain the penetration factor  $q_i$  of the Rayleigh wave. Because the SAW is expected to penetrate into the solid for  $z > 0$  during decay, we adopt the solution  $q$  with a positive value in the real part,  $q_{\text{Re}}$ , and a negative one in the imaginary part,  $q_{\text{Im}}$ , as

$$q = q_{\text{Re}} + iq_{\text{Im}} = 0.4311 - 0.5216i.\tag{13}$$

This solution gives the ratio  $\gamma$  as

$$\gamma = \gamma_{\text{Re}} + i\gamma_{\text{Im}} = -0.4311 - 1.1120i.\tag{14}$$

The corresponding  $u_x$  and  $u_z$  of the SAW of Eq. (4) are given as

$$\begin{aligned}u_x &= U \exp[-kqz + ik(x - vt)], \\ u_z &= -i\gamma u_x = 1.19 \exp[i\alpha]U \exp[-kqz + ik(x - vt)].\end{aligned}\tag{15}$$

Here, we have an angle of  $\alpha = 158.81^\circ$  for the phase shift of  $-i\gamma$ . The displacement components of  $u_x$  and  $u_z$  vary at the positions  $x$  and  $z$  and the time  $t$  with a phase velocity  $v = 4.844$  km/s along the  $x$ -direction. The real parts of  $u_x$  and  $u_z$  are written as

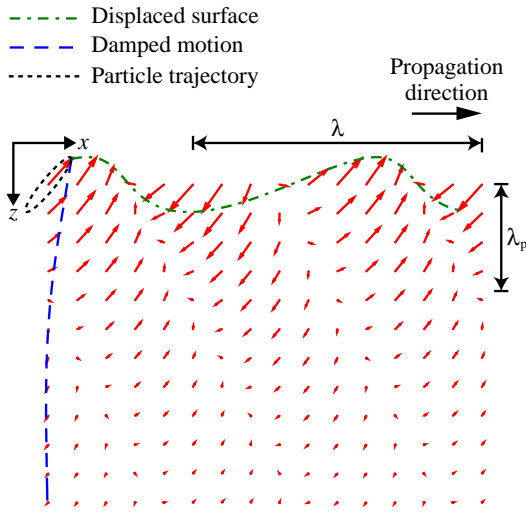


**Fig. 6.** (Color online) Instantaneous displacement components  $u_x$  and  $u_z$  of the SAW with a wavelength  $\lambda = 9.37 \mu\text{m}$  propagating along the  $x$ -axis on the  $z$  surface of the silicon wafer. The dot-dashed line denotes the displaced surface of the SAW. The dotted line denotes the ellipsoidal particle trajectory of  $u_z$  and  $u_x$  when penetrating into the  $z$ -axis on the silicon wafer with a penetration depth  $\lambda_p = 3.5 \mu\text{m}$ . The damped motion of  $u_x$  and  $u_z$  is shown by the dashed line.

$$\begin{aligned} u_x^{(\text{Re})} &= U \exp[-kq_{\text{Re}}z] \cos[k(x - vt) - kq_{\text{Im}}z], \\ u_z^{(\text{Re})} &= 1.19U \exp[-kq_{\text{Re}}z] \cos[k(x - vt) \\ &\quad - kq_{\text{Im}}z + 158.81^\circ]. \end{aligned} \quad (16)$$

The ellipsoidal trajectory of the instantaneous amplitude and directions of  $u_x$  and  $u_z$  in Eq. (16) is shown by arrows in Fig. 6. The dot-dashed line in Fig. 6 shows the displaced surface of  $u_x$  and  $u_z$  along the  $x$ -direction oscillating with a wavelength  $\lambda = 9.37 \mu\text{m}$  in the present SAW of  $f_s = 517 \text{MHz}$ . As shown in Fig. 6, the amplitude of  $u_x$  and  $u_z$  decreases to  $1/e$  when penetrating in the  $z$ -direction at a depth  $\lambda_p = \lambda/(2\pi q_{\text{Re}}) = 3.5 \mu\text{m}$  accompanied by an oscillation with a wavelength of  $\lambda_z = 2\pi/(k|q_{\text{Im}}|) = \lambda/|q_{\text{Im}}| = 18.0 \mu\text{m}$ .

In order to analyze the softening of the SAW in terms of the quadrupole-strain interaction in Sect. 4.2, we shall treat the symmetry strains  $\varepsilon_B$ ,  $\varepsilon_u$ , and  $\varepsilon_v$  defined as

$$\begin{aligned} \varepsilon_B &= \varepsilon_{xx} + \varepsilon_{yy} + \varepsilon_{zz} = \frac{\partial u_x}{\partial x} + \frac{\partial u_y}{\partial y} + \frac{\partial u_z}{\partial z}, \\ \varepsilon_u &= \frac{2\varepsilon_{zz} - \varepsilon_{xx} - \varepsilon_{yy}}{\sqrt{3}} = \frac{1}{\sqrt{3}} \left( 2 \frac{\partial u_z}{\partial z} - \frac{\partial u_x}{\partial x} - \frac{\partial u_y}{\partial y} \right), \\ \varepsilon_v &= \varepsilon_{xx} - \varepsilon_{yy} = \frac{\partial u_x}{\partial x} - \frac{\partial u_y}{\partial y}. \end{aligned} \quad (17)$$

Substituting Eq. (15) into Eqs. (2) and (17), we obtain the symmetry strains

$$\begin{aligned} \varepsilon_B &= ik(\gamma q + 1)u_x, \\ \varepsilon_u &= \frac{ik}{\sqrt{3}}(2\gamma q - 1)u_x, \\ \varepsilon_v &= iku_x, \\ \varepsilon_{yz} &= 0, \\ \varepsilon_{zx} &= k(\gamma - q)u_x, \\ \varepsilon_{xy} &= 0. \end{aligned} \quad (18)$$

Consequently, the Rayleigh wave of Eq. (15) propagating along the  $x$ -direction on the  $z$  surface of the silicon wafer

consists of the four symmetry strains  $\varepsilon_B$ ,  $\varepsilon_u$ ,  $\varepsilon_v$ , and  $\varepsilon_{zx}$ . The real parts of Eq. (18) are written as

$$\begin{aligned} \varepsilon_B^{(\text{Re})} &= A_B kU \exp[-kq_{\text{Re}}z] \cos[k(x - vt) - kq_{\text{Im}}z + \theta_B], \\ \varepsilon_u^{(\text{Re})} &= A_u kU \exp[-kq_{\text{Re}}z] \cos[k(x - vt) - kq_{\text{Im}}z + \theta_u], \\ \varepsilon_v^{(\text{Re})} &= A_v kU \exp[-kq_{\text{Re}}z] \cos[k(x - vt) - kq_{\text{Im}}z + \theta_v], \\ \varepsilon_{zx}^{(\text{Re})} &= A_{zx} kU \exp[-kq_{\text{Re}}z] \cos[k(x - vt) - kq_{\text{Im}}z + \theta_{zx}]. \end{aligned} \quad (19)$$

The numerical values  $q$  of Eq. (13) and  $\gamma$  of Eq. (14) give the sharing parameters in the amplitude  $A_{\Gamma_\gamma}$  (phase shift  $\theta_{\Gamma_\gamma}$ ) as  $A_B = 0.346$  ( $\theta_B = 42.61^\circ$ ),  $A_u = 1.491$  ( $\theta_u = 281.37^\circ$ ),  $A_v = 1.000$  ( $\theta_v = 90.00^\circ$ ), and  $A_{zx} = 1.045$  ( $\theta_{zx} = 214.41^\circ$ ).

Introducing a function of  $f_{\Gamma_\gamma}(z, x, t; \theta_{\Gamma_\gamma})$  depending on  $x$ ,  $z$ , and  $t$  with the phase shift  $\theta_{\Gamma_\gamma}$  as

$$f_{\Gamma_\gamma}(z, x, t; \theta_{\Gamma_\gamma}) = \exp[-kq_{\text{Re}}z] \cos[k(x - vt) - kq_{\text{Im}}z + \theta_{\Gamma_\gamma}], \quad (20)$$

we can write the symmetry strains  $\varepsilon_B$ ,  $\varepsilon_u$ ,  $\varepsilon_v$ , and  $\varepsilon_{zx}$  with the amplitude  $A_{\Gamma_\gamma}$  and phase shifts of  $\theta_{\Gamma_\gamma}$  of Eq. (19) as

$$\varepsilon_{\Gamma_\gamma}^{(\text{Re})} = A_{\Gamma_\gamma} f_{\Gamma_\gamma}(z, x, t; \theta_{\Gamma_\gamma}) \delta. \quad (21)$$

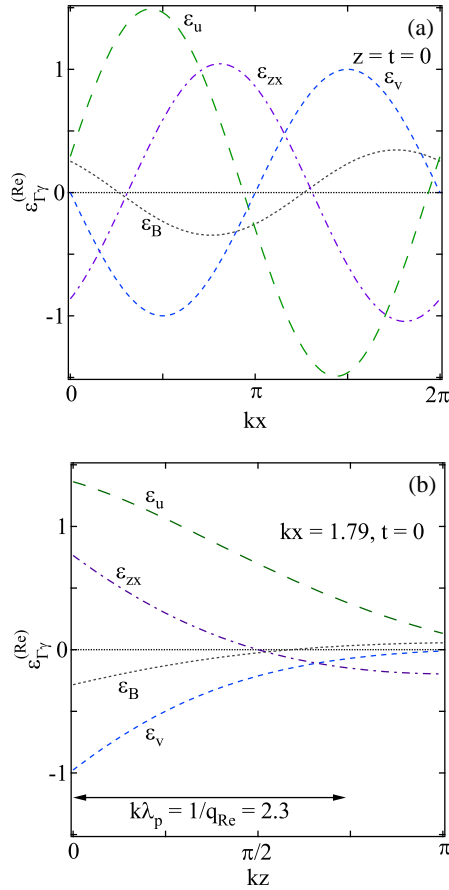
Here, an external perturbation parameter  $\delta = kU = 2\pi U/\lambda$ , proportional to the injection amplitude of the pulsed shape SAW, is introduced.

Figure 7(a) shows the instantaneous amplitude of the symmetry strains  $\varepsilon_B$ ,  $\varepsilon_u$ ,  $\varepsilon_v$ , and  $\varepsilon_{zx}$  of Eq. (19) along  $x$ -axis at  $z = 0$  and  $t = 0$ . The symmetry strains  $\varepsilon_u$  with the phase shift  $\theta_u = 281.37^\circ$  and  $\varepsilon_v$  with  $\theta_v = 90.00^\circ$  in Fig. 7(a) oscillate in keeping the almost antiphase relation  $|\theta_u - \theta_v| = 191.37^\circ$ . Furthermore, the symmetry strains  $\varepsilon_B$  with  $\theta_B = 42.61^\circ$  and  $\varepsilon_{zx}$  with  $\theta_{zx} = 214.41^\circ$  also share almost the antiphase relation  $|\theta_B - \theta_{zx}| = 171.80^\circ$ . This is caused by the fact that the SAW travels along the  $x$ -direction like a plane wave but considerably decays along the  $z$ -direction. The SAW located within the surface layer of  $\lambda_p$  is reminiscent of a stationary wave confined in an end-closed waveguide.

The instantaneous amplitude of the symmetry strains  $\varepsilon_B$ ,  $\varepsilon_u$ ,  $\varepsilon_v$ , and  $\varepsilon_{zx}$  along the penetrating  $z$ -direction for  $z > 0$  is shown in Fig. 7(b) for  $kx = 1.79$  and  $t = 0$ . The amplitude of an individual strain in Fig. 7(b) considerably decays along the  $z$ -direction as deep as  $k\lambda_p = 2\pi\lambda_p/\lambda = 1/q_{\text{Re}} = 2.3$ . The almost antiphase sharings between the symmetry strains  $\varepsilon_u$  and  $\varepsilon_v$  and between the strains  $\varepsilon_B$  and  $\varepsilon_{zx}$  are again observed in Fig. 7(b).

The total elastic energy  $U_{\text{total}}(z, x, t; \delta)$  depending on  $x$ ,  $z$ , and  $t$  associated with the SAW is written by the sum of the elastic energies  $U_B$ ,  $U_u$ ,  $U_v$ , and  $U_{zx}$ , which are caused by the symmetry strains  $\varepsilon_B$ ,  $\varepsilon_u$ ,  $\varepsilon_v$ , and  $\varepsilon_{zx}$ , respectively. Taking account of the symmetry strain  $\varepsilon_{\Gamma_\gamma}$  with the individual amplitude  $A_{\Gamma_\gamma}$  and the phase shift  $\theta_{\Gamma_\gamma}$ , we obtain the total elastic energy

$$\begin{aligned} U_{\text{total}}(z, x, t; \delta) &= \sum_{\Gamma_\gamma} \frac{1}{2} C_{\Gamma_\gamma} (\varepsilon_{\Gamma_\gamma}^{(\text{Re})})^2 \\ &= \sum_{\Gamma_\gamma} \frac{1}{2} C_{\Gamma_\gamma} \{A_{\Gamma_\gamma} f_{\Gamma_\gamma}(z, x, t; \theta_{\Gamma_\gamma})\}^2 \delta^2 \\ &= \frac{1}{2} C_B (A_B f_B(z, x, t; \theta_B))^2 \delta^2 \end{aligned}$$



**Fig. 7.** (Color online) (a) Instantaneous amplitude for the symmetry strains  $\varepsilon_B$ ,  $\varepsilon_u$ ,  $\varepsilon_v$ , and  $\varepsilon_{zx}$  induced by the SAW at the surface  $z = 0$  and time  $t = 0$ . The strains  $\varepsilon_B$  and  $\varepsilon_{zx}$ , and  $\varepsilon_u$  and  $\varepsilon_v$  oscillate in an almost antiphase manner relative to each other. This implies the stationary wave character of the SAW during decay along the  $z$ -axis with the penetration depth  $\lambda_p$ . (b) The instantaneous amplitude for the symmetry strains  $\varepsilon_B$ ,  $\varepsilon_u$ ,  $\varepsilon_v$ , and  $\varepsilon_{zx}$  induced by the SAW along the  $z > 0$  direction for  $kx = 1.79$  and  $t = 0$ .

$$\begin{aligned}
 & + \frac{1}{2} C_T (A_u f_u(z, x, t; \theta_u))^2 \delta^2 \\
 & + \frac{1}{2} C_T (A_v f_v(z, x, t; \theta_v))^2 \delta^2 \\
 & + \frac{1}{2} C_{44} (A_{zx} f_{zx}(z, x, t; \theta_{zx}))^2 \delta^2. \quad (22)
 \end{aligned}$$

Here, we abbreviate the elastic constant as  $C_T = (C_{11} - C_{12})/2$ .  $\sum_{\Gamma_\gamma}$  denotes the sum over the symmetry strains  $\varepsilon_B$ ,  $\varepsilon_u$ ,  $\varepsilon_v$ , and  $\varepsilon_{zx}$ . In Fig. 8(a), the instantaneous feature of the total elastic energy  $U_{\text{total}}(z, x, t; \delta)$  along the  $x$ -direction at  $z = 0$  and  $t = 0$  for the perturbation parameter  $\delta = kU = 1$  is shown together with the instantaneous energies caused by the symmetry strains. The total elastic energy  $U_{\text{total}}(z, x, t; \delta)$  of the SAW at  $t = 0$  in Fig. 8(a) shows its maximum for  $kx = 1.79$ .

Employing the power-reduction formula and linear combination of trigonometric functions, we can reduce the total energy  $U_{\text{total}}(z, x, t; \delta)$  in Eq. (22) to the time-dependent and time-independent parts of the elastic energies as

$$U_{\text{total}}(z, x, t; \delta) = \frac{1}{2} C_s^0 (|A_s| f_s(z, x, t; \theta_s))^2 \delta^2 + \frac{1}{2} K_0(z) \delta^2. \quad (23)$$

The former time-dependent energy means the part propagating along the  $x$ -direction, which is described in terms of the function

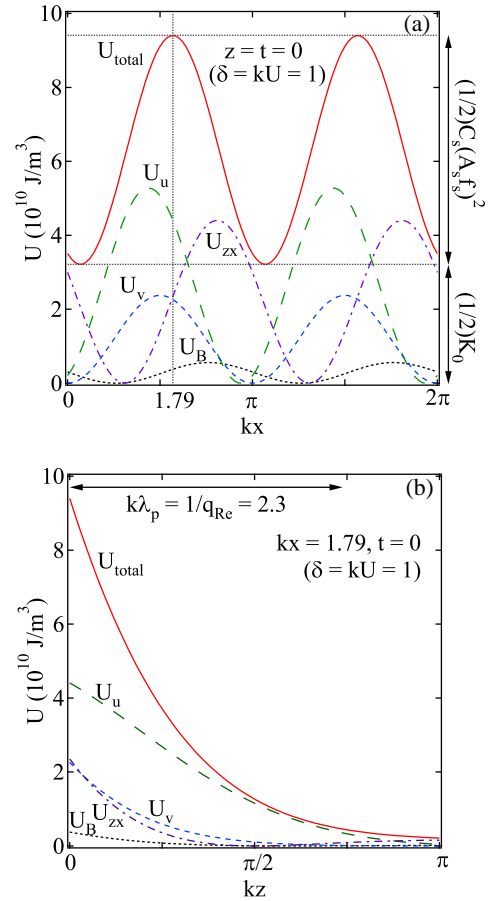


**Fig. 8.** (Color online) (a) Instantaneous elastic energy  $U_{\text{total}}$  of the SAW of Eq. (22) for  $\delta = kU = 1$  along the  $x$ -axis at the surface of  $z = 0$  and for time  $t = 0$  together with the elastic energies  $U_B$ ,  $U_u$ ,  $U_v$ , and  $U_{zx}$ . The  $U_{\text{total}}(x, z, t; \delta)$  of the SAW is described by the sum of the time-dependent and time-independent parts. (b) The instantaneous elastic energy  $U_{\text{total}}$  of the SAW penetrating in the  $z$ -direction for  $kx = 1.79$  and  $t = 0$  is shown together with the elastic energies  $U_B$ ,  $U_u$ ,  $U_v$ , and  $U_{zx}$  for  $\delta = kU = 1$ . The elastic energy shows a rapid decay with a penetration depth of  $k\lambda_p = 2.3$ .

$$\begin{aligned}
 & f_s(z, x, t; \theta_s) \\
 & = \exp[-kq_{\text{Re}}z] \cos[k(x - vt) + kq_{\text{Im}}z + \theta_s], \quad (24)
 \end{aligned}$$

and the amplitude

$$|A_s| = \sqrt{\frac{4\sqrt{g_c^2 + g_s^2}}{C_s^0}}. \quad (25)$$

The phase shift  $\theta_s$  of the SAW is represented by

$$\begin{aligned}
 \cos[2\theta_s] &= \frac{g_c}{\sqrt{g_c^2 + g_s^2}}, \\
 \sin[2\theta_s] &= \frac{g_s}{\sqrt{g_c^2 + g_s^2}}, \\
 g &= \frac{1}{4} \sum_{\Gamma_\gamma} C_{\Gamma_\gamma} A_{\Gamma_\gamma}^2, \\
 g_c &= \frac{1}{4} \sum_{\Gamma_\gamma} C_{\Gamma_\gamma} A_{\Gamma_\gamma}^2 \cos 2\theta_{\Gamma_\gamma}, \\
 g_s &= \frac{1}{4} \sum_{\Gamma_\gamma} C_{\Gamma_\gamma} A_{\Gamma_\gamma}^2 \sin 2\theta_{\Gamma_\gamma}. \quad (26)
 \end{aligned}$$

The latter time-independent energy denotes the non-propagating part along the penetrating  $z$ -direction. This is described by the function of

$$K_0(z) = 2(g - \sqrt{g_c^2 + g_s^2}) \exp[-2kq_{\text{Re}}z]. \quad (27)$$

The time-dependent elastic energy for the propagating part of the SAW is described by the square of  $A_s f_s(z, x, t; \theta_s) \delta$  for the amplitude  $|A_s| = 1.505$  and the phase  $\theta_s = 77.47^\circ$ . The time-independent elastic energy for the stationary wave is written as  $(1/2)K_0(z)\delta^2$  for  $K_0(z) = 6.428 \times 10^{10} \text{ J/m}^3$  at  $z = 0$ . The time-dependent and time-independent parts of the instantaneous energy of Eq. (23) for  $\delta = kU = 1$  at  $z = 0$  and  $t = 0$  are also pictured in Fig. 8(a). The Rayleigh wave shares out the amplitudes and phase shifts among the symmetry strains of Eq. (19) to minimize the time-dependent elastic energy of  $(1/2)C_s\{A_s f_s(z, x, t; \theta_s)\}^2 \delta^2$ .

Figure 8(b) shows the instantaneous feature of the total energy of  $U_{\text{total}}(z, x, t)$  and its symmetry parts of  $U_B$ ,  $U_u$ ,  $U_v$ , and  $U_{zx}$  in penetrating into the  $z$ -direction for  $z > 0$ . Here, we adopt the position of  $kx = 1.79$  and  $t = 0$  for  $\delta = kU = 1$ . The instantaneous energy of the SAW rapidly decays within the surface layer of the penetration depth of  $k\lambda_p = 2.3$ . The diagnostic application of the SAW guarantees for the vacancy evaluation within a surface layer as deep as  $\lambda_p = 3.5 \mu\text{m}$  of the silicon wafer. This prominent feature of the SAW measurement is definitely distinguished from the bulk ultrasonic measurement to evaluate the vacancy concentration of the inside of the wafer.

#### 4.2 Quadrupole susceptibility

The vacancy orbital of a charge state  $V^+$  in the boron-doped silicon wafer accommodates three electrons owing to charge neutrality, where one electron is released from the vacancy orbital to an acceptor state of the boron dopant. Four  $sp^3$  dangling bonds of  $\phi_i$  ( $i = 1, 2, 3, 4$ ) shown in Fig. 4 at a cubic site symmetry of  $T_d$  are lifted to a singlet  $a_1$  state with an energy of  $-3\gamma$  and a triplet  $t_2$  state with  $\gamma$  owing to the transfer energy of  $-\gamma = \langle \phi_j | H_0 | \phi_i \rangle$  ( $\gamma > 0$ ).<sup>24</sup> The energy gap of  $4\gamma \sim 1.7 \text{ eV} \sim 2.0 \times 10^4 \text{ K}$  between the singlet  $a_1$  state and the triplet  $t_2$  state was theoretically estimated.<sup>25,26</sup> The former singlet  $a_1$  state located beneath the top of the valence band accommodates two electrons with an antiparallel spin orientation, while the latter triplet  $t_2$  state located near the chemical potential possesses an electron with spin  $S = 1/2$ . The softening of the elastic constants of the silicon wafer measured by the bulk ultrasonic waves was successfully described in terms of the quadrupole susceptibility of the vacancy orbital.<sup>13,27,28</sup>

The magnetic field dependence of the elastic softening is responsible for the magnetism of the vacancy orbital accommodating three (odd) number electrons. The magnetism of the vacancy orbital is caused by the spin-orbit interaction of  $H_{\text{SO}} = \xi \mathbf{L} \cdot \mathbf{S}$  ( $\xi < 0$ ) of the electron with orbital  $L = 1$  and spin  $S = 1/2$  in the triplet  $t_2$  state. This  $H_{\text{SO}}$  gives rise to the  $\Gamma_8$  quartet ground state with the energy of  $\xi/2$  and the  $\Gamma_7$  excited state with the energy of  $-\xi$  as<sup>29</sup>

$$|\Gamma_7\rangle \left\{ \begin{array}{l} |\alpha\rangle = \sqrt{\frac{2}{3}} \left| 1, -\frac{1}{2} \right\rangle - \frac{1}{\sqrt{3}} \left| 0, \frac{1}{2} \right\rangle \\ |\beta\rangle = \sqrt{\frac{2}{3}} \left| -1, \frac{1}{2} \right\rangle - \frac{1}{\sqrt{3}} \left| 0, -\frac{1}{2} \right\rangle \end{array} \right.,$$

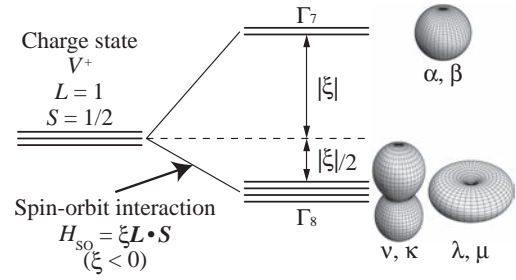


**Fig. 9.** The triplet  $t_2$  state with  $L = 1$  and  $S = 1/2$  of the charge state  $V^+$  of the vacancy orbital in boron-doped silicon forms the  $\Gamma_8$  quartet ground state ( $\nu$ ,  $\kappa$ ,  $\lambda$ , and  $\mu$ ) and  $\Gamma_7$  doublet excited state ( $\alpha$  and  $\beta$ ) due to the spin-orbit interaction  $H_{\text{SO}} = \xi \mathbf{L} \cdot \mathbf{S}$  ( $\xi < 0$ ). The  $\Gamma_8$ – $\Gamma_7$  states  $\nu$  and  $\kappa$ ,  $\lambda$  and  $\mu$ , and  $\alpha$  and  $\beta$  on the right-hand side have polar, donut, and spherical charge distribution, respectively.

$$|\Gamma_8\rangle \left\{ \begin{array}{l} |\nu\rangle = \frac{1}{\sqrt{3}} \left| 1, -\frac{1}{2} \right\rangle + \sqrt{\frac{2}{3}} \left| 0, \frac{1}{2} \right\rangle \\ |\kappa\rangle = \frac{1}{\sqrt{3}} \left| -1, \frac{1}{2} \right\rangle + \sqrt{\frac{2}{3}} \left| 0, -\frac{1}{2} \right\rangle \\ |\lambda\rangle = \left| 1, \frac{1}{2} \right\rangle \\ |\mu\rangle = \left| -1, -\frac{1}{2} \right\rangle \end{array} \right. \quad (28)$$

Here,  $|L_z, S_z\rangle$  means the state with angular momentum components over  $L_z = \pm 1, 0$  for  $L = 1$  and spin components over  $S_z = \pm 1/2$  for  $S = 1/2$ . The quadrupole susceptibilities for the vacancy orbital with  $\Gamma_8$  (0 K) and  $\Gamma_7$  (1 K) for the spin-orbit coupling of  $\xi = -2/3 \text{ K}$  well described the softening of the elastic constants measured by the bulk ultrasonic waves.<sup>14–16</sup>

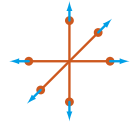
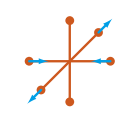
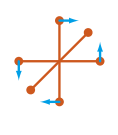
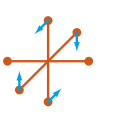
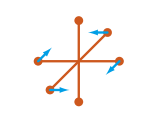
The spatial charge distribution distinguishes among three Kramers doublets of the vacancy orbital of Eq. (28). As shown in Fig. 9, the Kramers doublet of  $\nu$  and  $\kappa$  in the  $\Gamma_8$  quartet shows a polar charge distribution elongating along the  $z$ -axis, while the Kramers doublet of  $\lambda$  and  $\mu$  bears a donut-type distribution spreading in the  $x$ – $y$  plane. The  $\Gamma_7$  Kramers doublet of  $\alpha$  and  $\beta$  has a spherical charge distribution. The characteristic charge distribution in the  $\Gamma_8$ – $\Gamma_7$  states of the vacancy orbital is responsible for the coupling between the electric quadrupoles and the symmetry strains associated with the SAW.

It is known that the  $\Gamma_8$  quartet has three magnetic dipoles, five electric quadrupoles, and seven magnetic octupoles.<sup>30</sup> Among them, the electric quadrupoles couple to the elastic strains associated with ultrasonic waves. Actually, the considerable elastic softening with decreasing temperature was observed in  $\text{CeB}_6$ <sup>31,32</sup> and  $\text{Ce}_3\text{Pd}_{20}\text{Ge}_6$ <sup>33</sup>) with the  $\Gamma_8$  quartet ground state. The coupling between the electric quadrupoles of the  $\Gamma_8$  quartet ground state of the vacancy orbital and the elastic strains of the SAW is relevant for the description of the softening of  $C_s$ .

The applied magnetic fields of  $\mathbf{H}$  lift the Kramers doublets of the vacancy orbital. This is caused by the Zeeman energy as

$$H_{\text{Zeeman}} = \mu_B (\mathbf{L} + 2\mathbf{S}) \cdot \mathbf{H}. \quad (29)$$

Here,  $\mu_B = e\hbar/(2mc) \sim 0.67 \text{ K/T}$  is the Bohr magneton. Among the two Kramers doublets of the  $\Gamma_8$  quartet ground

Irrep $\Gamma$	$\Gamma_1$	$\Gamma_3$		$\Gamma_5$		
Electric Multipole $O_{\Gamma_Y}$	 $H_0$	 $O_u = \frac{2L_z^2 - L_x^2 - L_y^2}{\sqrt{3}}$	 $O_v = L_x^2 - L_y^2$	 $O_{yz} = L_y L_z + L_z L_y$	 $O_{cx} = L_z L_x + L_x L_z$	 $O_{xy} = L_x L_y + L_y L_x$
Elastic Strain $\epsilon_{\Gamma_Y}$	 $\epsilon_B = \epsilon_{xx} + \epsilon_{yy} + \epsilon_{zz}$	 $\epsilon_u = \frac{2\epsilon_{zz} - \epsilon_{xx} - \epsilon_{yy}}{\sqrt{3}}$	 $\epsilon_v = \epsilon_{xx} - \epsilon_{yy}$	 $\epsilon_{yz}$	 $\epsilon_{cx}$	 $\epsilon_{xy}$
Elastic Constant $C_{\Gamma_Y}$	$C_B = \frac{C_{11} + 2C_{12}}{3}$	$C_T = \frac{C_{11} - C_{12}}{2}$		$C_{44}$		

**Fig. 10.** (Color online) Electric multipoles, counterpart symmetry strains, and corresponding elastic constants. The quadrupole-strain interaction for the vacancy orbital brings about the softening of the elastic constant  $C_s$ .  $H_0$  means the electric hexadecapole described by the  $\Gamma_1$ -irreducible representation (irrep).

state, the  $\nu$  and  $\kappa$  states with magnetic moments of  $\pm(2/3)\mu_B$  and  $\lambda$  and  $\mu$  states with  $\pm 2\mu_B$  are distinct from each other at magnetic fields along the  $z$ -axis. The  $\Gamma_7$  Kramers doublet state  $\alpha$  and  $\beta$  have different magnetic moments of  $\pm(1/3)\mu_B$ . In the present experiments, we applied the magnetic fields along the  $x$ -axis parallel to the propagating direction of the SAW. The corresponding Zeeman energy  $H_{\text{Zeeman}} = \mu_B(L_x + 2S_x)H_x$  is responsible for the magnetic field effects of the elastic constant  $C_s$  of the present SAW measurements on the silicon wafer.

The coupling between the electric monopole and the volume strain  $\epsilon_B$  with the full symmetry  $\Gamma_1$  is relevant for the valence instability system like  $\text{SmB}_6$ .<sup>34</sup> Because the charge state  $V^+$  of the boron-doped silicon is stable, the coupling between the electric monopole and  $\epsilon_B$  seems to be irrelevant. The coupling between the higher order electric hexadecapole  $H_0 = 35L_z^4 - \{30L(L+1) - 25\}L_z^2 + 3L^2(L+1)^2 - 6L(L+1) + (5/2)(L_+^4 + L_-^4)$  and the volume strain  $\epsilon_B$  is principally possible in the highly degenerate  $\Gamma_8$ - $\Gamma_7$  states. The present analysis, however, excludes it because of its negligible contribution to the softening. We restrict ourselves to the coupling between the symmetry breaking strains associated with the SAW and the appropriate electric quadrupoles of the vacancy orbital.

The softening of  $C_s$  of the SAW down to the base temperature of 23 mK in Fig. 4 is accounted for in terms of the quadrupole susceptibility for the vacancy orbital, which is located in the surface layer within the penetration depth of  $\lambda_p$ . The scalar potential energy  $V$  of the vacancy orbital is modulated by the elastic strains of the SAW as  $V = V_0 + \sum_{\Gamma_Y} (\partial V / \partial \epsilon_{\Gamma_Y}^{(\text{Re})}) \epsilon_{\Gamma_Y}^{(\text{Re})}$ . Here,  $V_0$  denotes an unperturbed potential energy. The derivative of  $\partial V / \partial \epsilon_{\Gamma_Y}^{(\text{Re})}$  is represented by the electric quadrupole  $O_{\Gamma_Y}$ , which is written by the symmetry square of the Cartesian coordinates  $x$ ,  $y$ , and  $z$ , and the quadrupole-strain coupling constant  $g_{\Gamma}$ . Therefore, the

perturbation energy due to the elastic strains of the SAW is written by the quadrupole-strain interaction  $H_{\text{QS}}$  as<sup>35,36</sup>

$$H_{\text{QS}} = g_{\Gamma_3}(O_u \epsilon_u^{(\text{Re})} + O_v \epsilon_v^{(\text{Re})}) + g_{\Gamma_5} O_{zx} \epsilon_{zx}^{(\text{Re})}. \quad (30)$$

The eigenfunctions of the  $\Gamma_8$ - $\Gamma_7$  states of the vacancy orbital of Eq. (28) are represented by the quantum numbers of  $L_z$  and  $S_z$ . Taking account of the Wigner-Eckert theorem,<sup>37</sup> we can write the electric quadrupoles using the symmetry square of the orbital angular momentum operators of  $L_x$ ,  $L_y$ , and  $L_z$ . We adopt the electric quadrupoles of  $O_u = (2L_z^2 - L_x^2 - L_y^2)/\sqrt{3}$  and  $O_v = L_x^2 - L_y^2$  with the  $\Gamma_3$ -irreducible representation and  $O_{zx} = L_z L_x + L_x L_z$  with the  $\Gamma_5$ -irreducible representation. In Fig. 10, we list the electric quadrupoles (multipoles) and the counterpart symmetry strains in the quadrupole-strain interaction of the cubic system.

The perturbation energy  $E_i(\epsilon_{\Gamma_Y}^{(\text{Re})})$  for the  $i$ th state ( $i = \alpha, \beta, \nu, \kappa, \lambda, \mu$ ) of the vacancy orbital consisting of the  $\Gamma_8$ - $\Gamma_7$  states is calculated using the perturbation Hamiltonian  $H_{\text{QS}} = g_{\Gamma} O_{\Gamma_Y} \epsilon_{\Gamma_Y}^{(\text{Re})}$  for the appropriate symmetry strain of  $\epsilon_{\Gamma_Y}^{(\text{Re})}$  as

$$E_i(\epsilon_{\Gamma_Y}^{(\text{Re})}) = E_i^0 + g_{\Gamma} \langle i | O_{\Gamma_Y} | i \rangle \epsilon_{\Gamma_Y}^{(\text{Re})} + g_{\Gamma}^2 \sum_{j(\neq i)} \frac{|\langle i | O_{\Gamma_Y} | j \rangle|^2}{E_i^0 - E_j^0} (\epsilon_{\Gamma_Y}^{(\text{Re})})^2. \quad (31)$$

Here,  $E_i^0$  denotes the unperturbed energy of the  $i$ th state of the vacancy orbital of Eq. (28).

The total free energy of the system consisting of the vacancy orbital with the vacancy concentration  $N$  in the surface layer of the silicon wafer is written as

$$F(\epsilon_{\Gamma_Y}^{(\text{Re})}) = \frac{1}{2} C_{\Gamma_Y}^0 (\epsilon_{\Gamma_Y}^{(\text{Re})})^2 - N k_B T \ln \left[ \sum_i \exp \left[ -\frac{E_i(\epsilon_{\Gamma_Y}^{(\text{Re})})}{k_B T} \right] \right]. \quad (32)$$

The second derivative of the free energy with respect to the symmetry strain  $\varepsilon_{\Gamma_\gamma}^{(\text{Re})}$  leads to the elastic constant  $C_{\Gamma_\gamma}$  as

$$C_{\Gamma_\gamma} = \frac{\partial^2 F}{\partial \varepsilon_{\Gamma_\gamma}^{(\text{Re})2}} = C_{\Gamma_\gamma}^0 - Ng_{\Gamma_\gamma}^2 \chi(O_{\Gamma_\gamma}). \quad (33)$$

Here, the quadrupole susceptibility  $-\chi(O_{\Gamma_\gamma})$  for the electric quadrupole  $O_{\Gamma_\gamma}$  is defined as<sup>7,8,35</sup>

$$\chi(O_{\Gamma_\gamma}) = \sum_{\substack{i,j \\ E_i^0 \neq E_j^0}} \frac{n_j - n_i}{E_i^0 - E_j^0} |\langle i|O_{\Gamma_\gamma}|j \rangle|^2 + \frac{1}{k_B T} \left[ \sum_i |\langle i|O_{\Gamma_\gamma}|i \rangle|^2 n_i - \left( \sum_i |\langle i|O_{\Gamma_\gamma}|i \rangle| n_i \right)^2 \right]. \quad (34)$$

Here,  $n_i = Z^{-1} \exp[-E_i^0/k_B T]$  is the Boltzmann occupation probability with the partition function  $Z = \sum_i \exp[-E_i^0/k_B T]$ . On the analogy of the magnetic susceptibility, the

first term on the right-hand side of Eq. (34) denotes the van Vleck term associated with off-diagonal processes and the second term is the Curie term associated with the diagonal processes. The former van Vleck term leads to the temperature-independent softening, while the latter Curie term brings about the steep softening proportional to the reciprocal temperature. The quadrupole interaction among the vacancy orbitals at different sites is excluded in the present analysis, because the strong quadrupole-strain interaction dominates the low-temperature softening of the system and the intersite quadrupole interaction scarcely contributes to the softening.<sup>15)</sup>

In order to explain the appreciable softening of  $C_s$  caused by the Curie term of Eq. (34), we present the matrix elements  $\langle i|O_{\Gamma_\gamma}|j \rangle$  of the electric quadrupoles  $O_u$ ,  $O_v$ , and  $O_{zx}$  for the  $\Gamma_8$ - $\Gamma_7$  states of the vacancy orbital in Eq. (28) at zero magnetic field as

$$\begin{aligned} \langle i|O_u|j \rangle &= \frac{1}{\sqrt{3}} \begin{pmatrix} \alpha & \beta & \nu & \kappa & \lambda & \mu \\ \alpha & 0 & 0 & \sqrt{2} & 0 & 0 \\ \beta & 0 & 0 & 0 & \sqrt{2} & 0 \\ \nu & \sqrt{2} & 0 & -1 & 0 & 0 \\ \kappa & 0 & \sqrt{2} & 0 & -1 & 0 \\ \lambda & 0 & 0 & 0 & 0 & 1 \\ \mu & 0 & 0 & 0 & 0 & 0 \end{pmatrix}, & \langle i|O_v|j \rangle &= \frac{1}{\sqrt{3}} \begin{pmatrix} \alpha & \beta & \nu & \kappa & \lambda & \mu \\ \alpha & 0 & 0 & 0 & 0 & \sqrt{2} \\ \beta & 0 & 0 & 0 & \sqrt{2} & 0 \\ \nu & 0 & 0 & 0 & 0 & 1 \\ \kappa & 0 & 0 & 0 & 1 & 0 \\ \lambda & 0 & \sqrt{2} & 0 & 1 & 0 \\ \mu & \sqrt{2} & 0 & 1 & 0 & 0 \end{pmatrix}, \\ \langle i|O_{zx}|j \rangle &= \frac{1}{\sqrt{3}} \begin{pmatrix} \alpha & \beta & \nu & \kappa & \lambda & \mu \\ \alpha & 0 & 0 & 0 & \sqrt{\frac{3}{2}} & -\frac{1}{\sqrt{2}} \\ \beta & 0 & 0 & -\sqrt{\frac{3}{2}} & 0 & \frac{1}{\sqrt{2}} \\ \nu & 0 & -\sqrt{\frac{3}{2}} & 0 & 0 & 1 \\ \kappa & \sqrt{\frac{3}{2}} & 0 & 0 & 0 & -1 \\ \lambda & -\frac{1}{\sqrt{2}} & 0 & 1 & 0 & 0 \\ \mu & 0 & \frac{1}{\sqrt{2}} & 0 & -1 & 0 \end{pmatrix}. \end{aligned} \quad (35)$$

The electric quadrupoles  $O_u$ ,  $O_v$ , and  $O_{zx}$  commonly have diagonal elements for the  $\nu$ ,  $\kappa$ ,  $\lambda$ , and  $\mu$  of the  $\Gamma_8$  quartet ground state, but no elements for the  $\alpha$  and  $\beta$  of the  $\Gamma_7$  doublet excited state. The lifting of the  $\Gamma_8$  quartet ground state to two Kramers doublets due to the quadrupole-strain interaction in Eq. (30) brings about the softening of the elastic constant due to the Curie term in Eq. (34). The off-diagonal elements of  $O_u$ ,  $O_v$ , and  $O_{zx}$  between the  $\Gamma_8$  quartet ground state and  $\Gamma_7$  doublet excited state in Eq. (35) lead to the van Vleck term in Eq. (34).

For accurate calculations of the low-temperature softening of  $C_s$ , we explain the perturbation Hamiltonian of Eq. (30) using the time-dependent symmetry strains of Eq. (21) induced by the SAW as

$$\begin{aligned} H_{\text{QS}} &= \sum_{\Gamma_\gamma} g_{\Gamma_\gamma} O_{\Gamma_\gamma} \varepsilon_{\Gamma_\gamma}^{(\text{Re})} \\ &= \sum_{\Gamma_\gamma} g_{\Gamma_\gamma} O_{\Gamma_\gamma} A_{\Gamma_\gamma} f_{\Gamma_\gamma}(z, x, t; \theta_{\Gamma_\gamma}) \delta \\ &= g_{\Gamma_3} O_u A_u f_u(z, x, t; \theta_u) \delta + g_{\Gamma_3} O_v A_v f_v(z, x, t; \theta_v) \delta \\ &\quad + g_{\Gamma_5} O_{zx} A_{zx} f_{zx}(z, x, t; \theta_{zx}) \delta. \end{aligned} \quad (36)$$

Taking account of the quadrupole-strain interaction of Eq. (36), the perturbation energy for the vacancy orbital is calculated up to the second-order processes of the external perturbation  $\delta$  using Eq. (31). Here, the matrix elements of the electric quadrupoles of Eq. (35) are employed.

The total elastic energy  $U_{\text{total}}$  of Eqs. (22) and (23) for the SAW is renormalized by the quadrupole-strain interaction of Eq. (36) as

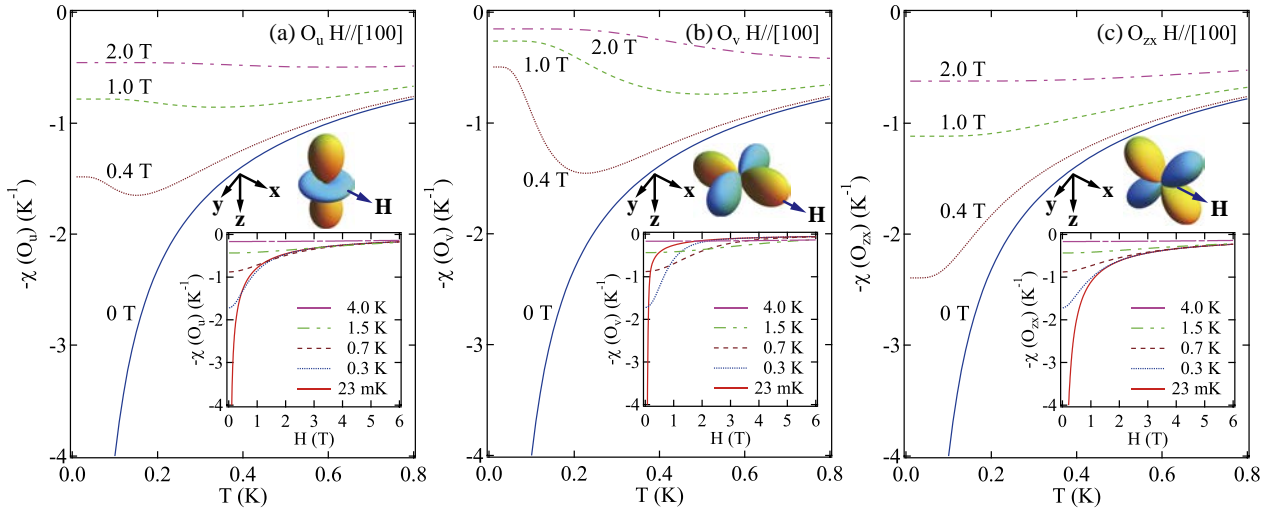


**Fig. 11.** (Color online) Temperature dependences of the quadrupole susceptibilities  $-\chi(O_u)$  in (a),  $-\chi(O_v)$  in (b), and  $-\chi(O_{zx})$  in (c) under applied the magnetic fields of  $\mathbf{H} = (H_x, 0, 0)$  parallel to the propagation direction of the SAW. The anisotropic charge distribution of the electric quadrupoles is also presented. The inset shows the magnetic field dependences of the quadrupole susceptibilities at low temperatures.

$$\begin{aligned}
 U_{\text{total}} &= \frac{1}{2} C_s (A_s f_s(z, x, t; \theta_s))^2 \delta^2 + \frac{1}{2} K_0(z) \delta^2 \\
 &= \frac{1}{2} C_B (A_B f_B(z, x, t; \theta_B))^2 \delta^2 \\
 &+ \frac{1}{2} (C_T - N g_{\Gamma_3}^2 \chi(O_u)) (A_u f_u(z, x, t; \theta_u))^2 \delta^2 \\
 &+ \frac{1}{2} (C_T - N g_{\Gamma_3}^2 \chi(O_v)) (A_v f_v(z, x, t; \theta_v))^2 \delta^2 \\
 &+ \frac{1}{2} (C_{44} - N g_{\Gamma_5}^2 \chi(O_{zx})) (A_{zx} f_{zx}(z, x, t; \theta_{zx}))^2 \delta^2. \quad (37)
 \end{aligned}$$

The second derivative of the elastic energy of the SAW of Eq. (37) with respect to the external perturbation  $\delta$  gives the softening and its magnetic field dependence on the renormalized elastic constant  $C_s$  of the SAW as

$$\begin{aligned}
 \frac{\partial^2 U_{\text{total}}}{\partial \delta^2} &= C_s (A_s f_s(z, x, t; \theta_s))^2 + K_0(z) \\
 &= C_B (A_B f_B(z, x, t; \theta_B))^2 \\
 &+ (C_T - N g_{\Gamma_3}^2 \chi(O_u)) (A_u f_u(z, x, t; \theta_u))^2 \\
 &+ (C_T - N g_{\Gamma_3}^2 \chi(O_v)) (A_v f_v(z, x, t; \theta_v))^2 \\
 &+ (C_{44} - N g_{\Gamma_5}^2 \chi(O_{zx})) (A_{zx} f_{zx}(z, x, t; \theta_{zx}))^2. \quad (38)
 \end{aligned}$$

The temperature dependence of  $C_s$  shown in Fig. 4 and the magnetic field dependence of  $C_s$  shown in Fig. 5(a) are explained in terms of the quadrupole susceptibilities  $-\chi(O_u)$ ,  $-\chi(O_v)$ , and  $-\chi(O_{zx})$  as

$$\begin{aligned}
 C_s &= C_s^0 - \frac{N}{(A_s f_s(z, x, t; \theta_s))^2} [g_{\Gamma_3}^2 (A_u f_u(z, x, t; \theta_u))^2 \chi(O_u) \\
 &+ g_{\Gamma_3}^2 (A_v f_v(z, x, t; \theta_v))^2 \chi(O_v) \\
 &+ g_{\Gamma_5}^2 (A_{zx} f_{zx}(z, x, t; \theta_{zx}))^2 \chi(O_{zx})]. \quad (39)
 \end{aligned}$$

Here, the quadrupole susceptibilities of  $-\chi(O_u)$ ,  $-\chi(O_v)$ , and  $-\chi(O_{zx})$  as functions of temperature and magnetic field along the  $x$ -direction are shown in Figs. 11(a)–11(c), respectively.  $C_s^0$  is the background elastic constant where the quadrupole-strain interaction is ignored as

$$\begin{aligned}
 C_s^0 &= (A_s f_s(z, x, t; \theta_s))^2 \\
 &= C_B (A_B f_B(z, x, t; \theta_B))^2 + C_T (A_u f_u(z, x, t; \theta_u))^2 \\
 &+ C_T (A_v f_v(z, x, t; \theta_v))^2 + C_{44} (A_{zx} f_{zx}(z, x, t; \theta_{zx}))^2 \\
 &- K_0(z). \quad (40)
 \end{aligned}$$

$C_s^0$  is expected to faintly increase with decreasing temperature because of anharmonic vibrations of the Rayleigh wave.

## 5. Discussion

In order to fit the softening and its magnetic field dependence on  $C_s$  by Eq. (39), we need numerical values of the quadrupole-strain coupling constants of  $g_{\Gamma_3}$  and  $g_{\Gamma_5}$  in Eq. (30). Recently, the authors' group has reported the sum rule between the number of the vacancies consumed in the void formation and the number of residual vacancies proportional to the low-temperature softening of the  $C_{44}$  of the bulk transverse ultrasonic wave.<sup>16</sup> This sum rule leads to a strong coupling constant of  $g_{\Gamma_5} = 2.8 \times 10^5$  K between the electric quadrupole of  $O_{zx}$  and the counterpart symmetry strain of  $\varepsilon_{zx}$  in Eq. (30). Namely, the deformation energy for the external strain of  $\varepsilon_{zx} = 1$  corresponds to  $g_{\Gamma_5} \langle \Gamma_8 | O_{zx} | \Gamma_8 \rangle = 2.8 \times 10^5 / \sqrt{3}$  K =  $1.6 \times 10^5$  K = 14 eV. Furthermore, the ratio of  $g_{\Gamma_5} / g_{\Gamma_3} = 1.6$  was deduced by measuring of the relative amount of the low-temperature softening of both elastic constants  $C_{44}$  and  $(C_{11} - C_{12})/2$ .<sup>15</sup> Using the coupling constants  $g_{\Gamma_5} = 2.8 \times 10^5$  K and  $g_{\Gamma_3} = 1.8 \times 10^5$  K and the amplitude  $A_{\Gamma_\gamma}$  and the phase  $\theta_{\Gamma_\gamma}$  in the function  $f_{\Gamma_\gamma}(z, x, t; \theta_{\Gamma_\gamma})$  of Eq. (19) in Sect. 4.1, we have made a fit for the softening of  $C_s$  by the solid line in Fig. 4. We have deduced the vacancy concentration  $N = 3.1 \times 10^{12}/\text{cm}^3$  in the surface layer within  $\lambda_p = 3.5 \mu\text{m}$  of the present silicon wafer. In the fitting, we simply offset the extrinsic phase shift at a superconducting transition temperature of 1.17 K of the Al electrode to continue on both sides. Furthermore, we adopted the temperature-dependent background of the elastic constant in Eq. (40) described by  $C_s^0 = C^0 - a / (\exp[b/T] - 1)$  with the parameters  $C^0 = 5.749 \times 10^{10}$  J/m<sup>3</sup>,  $a = 6.30 \times 10^6$  J/m<sup>3</sup>, and  $b = 7.3$  K. The dashed line in Fig. 4 shows the background.

The magnetic fields applied parallel to the propagating  $x$ -direction of the SAW reduce the low-temperature softening of  $C_s$ . As shown in Figs. 5(a) and 5(b), the softening of  $C_s$  is completely suppressed at magnetic fields of up to 2.0 T. This is due to the lifting of the Kramers doublets of the  $\Gamma_8$ – $\Gamma_7$  states by the Zeeman energy in Eq. (29). The magnetic field dependences of the quadrupole susceptibilities  $-\chi(O_u)$ ,  $-\chi(O_v)$ , and  $-\chi(O_{zx})$  under the fields along the  $x$ -direction of up to 6 T for various temperatures are shown in Figs. 11(a)–11(c), respectively. The configurations between the electric quadrupole and the applied field direction along the  $x$ -direction are also shown in Fig. 11. Furthermore, the insets of Figs. 11(a)–11(c) show the magnetic field dependence of the quadrupole susceptibilities of  $-\chi(O_u)$ ,  $-\chi(O_v)$ , and  $-\chi(O_{zx})$ , respectively, up to 6 T. The magnetic fields along the  $x$ - and  $z$ -directions give the same effects on the unperturbed  $\Gamma_8$ – $\Gamma_7$  states of the vacancy orbital at the cubic site symmetry. When we treat the quadrupole-strain interaction of Eqs. (30) and (36) for the SAW propagating along the  $x$ -direction on the  $z$  surface, the present magnetic field along the  $x$ -direction affects the softening differently from that along the  $z$ -direction. The solid and dashed lines in Fig. 5(b) are fits for the softening and its field dependence on  $C_s$  in terms of the quadrupole susceptibilities in Eq. (34). The results of the theoretical calculations of  $C_s$  in Fig. 5(b) using the quadrupole susceptibilities are in fair agreement with those of the SAW experiments on  $C_s$  in Fig. 5(a).

Despite the fairly good consistency between the results of the SAW experiments and calculations based on the vacancy orbital with the  $\Gamma_8$ – $\Gamma_7$  states, the softening of  $C_s$  below 0.1 K in the zero magnetic field in Fig. 5(b) slightly deviates from the theory. Because of the strong quadrupole-strain coupling constants  $g_{\Gamma_3} = 1.8 \times 10^5$  K for the symmetry strains  $\varepsilon_u$  and  $\varepsilon_v$  and  $g_{\Gamma_5} = 2.8 \times 10^5$  K for  $\varepsilon_{zx}$ , even a tiny strain of  $\varepsilon \sim 10^{-6}$  may lift the  $\Gamma_8$  quartet ground state to two Kramers doublets with an order of energy of 0.1 K. Although we have attempted to eliminate unwanted strains, tiny strains might still remain in the silicon sample. This may give rise to the lifting of the  $\Gamma_8$  ground state, which plausibly accounts for the slight deviation in the softening of  $C_s$  from the theory. The precise measurement of the low-temperature softening of  $C_s$  as a function of externally applied stress acting on silicon samples is reserved for future work to verify the strain-sensitive feature of the vacancy orbital with the  $\Gamma_8$  ground state.

## 6. Conclusions

Focusing on boron-doped silicon wafers currently available for the fabrication of semiconductor devices, we have measured SAWs propagating on the surface of the wafer. An IDT with a comb gap of  $w = 2.5 \mu\text{m}$  optimally generated a SAW of  $f_s = 517$  MHz. A pulsed shape SAW propagates along the  $x$ -direction with a group velocity  $v_s = 4.967$  km/s and a wavelength  $\lambda_s = v_s/f_s = 9.61 \mu\text{m} \sim 4w = 10 \mu\text{m}$ . The equations of motion for the SAW on the  $z$  surface of the silicon wafer give the Rayleigh wave with a velocity  $v = 4.844$  km/s, which is in agreement with the observed SAW velocity  $v_s = 4.967$  km/s. The SAW with the ellipsoidal trajectory of the displacement components  $u_x$  and  $u_z$  induces the time-dependent symmetry strains  $\varepsilon_B$ ,  $\varepsilon_u$ ,  $\varepsilon_v$ , and  $\varepsilon_{zx}$  with the different amplitude and phase shifts. The

almost anti-phase relations between  $\varepsilon_B$  and  $\varepsilon_{zx}$  and between  $\varepsilon_u$  and  $\varepsilon_v$  indicate the stationary wave character of the SAW during decay along the penetrating  $z$ -direction.

The remarkable softening of  $\Delta C_s/C_s = 1.9 \times 10^{-4}$  below 2 K down to a base temperature of 23 mK is caused by the coupling between the SAW and the vacancy orbital with the  $\Gamma_8$  ground state and  $\Gamma_7$  excited state located at 1 K. Magnetic fields of up to 2 T fully suppress the softening of the SAW due to the lifting of the  $\Gamma_8$ – $\Gamma_7$  states at the magnetic fields. The low-temperature softening and its magnetic field dependence are well described in terms of the quadrupole susceptibilities based on the coupling between the symmetry strains  $\varepsilon_u$ ,  $\varepsilon_v$ , and  $\varepsilon_{zx}$  of the SAW and the appropriate electric quadrupoles. Taking account of the strong quadrupole-strain interactions of  $g_{\Gamma_5} = 2.8 \times 10^5$  K and  $g_{\Gamma_3} = 1.8 \times 10^5$  K for the vacancy orbital, we deduced the low vacancy concentration  $N = 3.1 \times 10^{12}/\text{cm}^3$  in the surface layer within a penetration depth  $\lambda_p = 3.5 \mu\text{m}$  of the silicon wafer. The present result promises a highly sensitive diagnostic tool of the SAW where the softening of  $\Delta C_s/C_s = 1.0 \times 10^{-4}$  corresponds to a vacancy concentration  $N = 1.6 \times 10^{12}/\text{cm}^3$  in the surface layer. The advantage of the SAW is clearly seen as compared with sensitivity of the bulk transverse ultrasonic wave measurement where the softening of  $\Delta C_{44}/C_{44} = 1.0 \times 10^{-4}$  corresponds to  $N = 1.5 \times 10^{13}/\text{cm}^3$  in the bulk region of the wafer.<sup>16)</sup>

The complementary metal oxide semiconductor is widely adopted in the fabrication of various large-scale integrated (LSI) devices of center processing units, dynamic random access memories, NAND-type flash memories, and charge couple devices to name a few.<sup>38,39)</sup> The active region beneath the surface of the silicon wafer in the depth range of 1–3  $\mu\text{m}$  is particularly utilized in LSI device fabrication. The vacancies play important roles in the proper control of a diffusion of dopants, precipitation of bulk micro-defects, and gettering of metal impurities in device fabrication. Therefore, the vacancy evaluation in the surface layer of silicon wafers is crucially required for the fabrication of the high-density LSI devices beyond 19 nm in size in order to obtain a high yield. The continuous pursuit of the high-quality wafers of polished, annealed, and epitaxial types with 450 mm as well as 300 mm in diameter demands the fine control of the vacancy concentration in the surface layer. The low-temperature measurement of the SAW demonstrated in the present study surely suggests an innovative technology for determining the vacancy concentration in the surface layer, which is one of the figure merits of the use of silicon wafers.

## Acknowledgments

We thank Akira Hasegawa and Takehiko Bando of Niigata University, Masashi Muromachi and Syouzou Saito of Toshiba Corporation, and Susumu Kouyama of GlobalWafers Japan Co., Ltd., for continuously supporting basic research in pursuit of an innovative technology for vacancy evaluation. We also thank Akira Yoshihara of Ishinomaki Senshu University for illuminative discussions of the SAW, Haruhiko Suzuki of Kanazawa University for the low-temperature SAW measurements in magnetic fields, and Yoshio Satoh of Taiyo Yuden Co., Ltd., for valuable suggestions regarding the IDT fabrication on the wafer. This work was supported by a Grant-in-Aid for Specially Promoted Research

(No. 18002008) “Strongly correlated quantum phases associated with charge fluctuations” from the Ministry of Education, Culture, Sports, Science and Technology of Japan. The present work was also supported by the Innovation Research Project on Nanoelectronics Materials and Structure from the Ministry of Economy, Trade and Industry of Japan (NEDO). We appreciate the support in the form of a Grant-in-Aid for Scientific Research “Supporting Program for Creating University Ventures” from the Japan Science and Technology Agency (JST). We also appreciate the support through the Strategic Young Researcher Overseas Visits Program for Accelerating Brain Circulation from the Japan Society for the Promotion of Science (JSPS).

\*goto@phys.sc.niigata-u.ac.jp

- 1) L. Rayleigh, *Proc. London Math. Soc.* **s1-17**, 4 (1885).
- 2) J. C. Irvin, *Bell Syst. Tech. J.* **41**, 387 (1962).
- 3) A. A. Oliner, *Acoustic Surface Wave, Topics in Applied Physics* (Springer, Berlin, 1978) Vol. 24, Chap. 3, p. 61.
- 4) Y. Satoh and O. Ikata, *Int. J. High Speed Electron. Syst.* **10**, 825 (2000).
- 5) D. Morgan, *Surface Acoustic Wave Filters* (Academic Press, New York, 2007) 2nd ed., Chap. 1, p. 1.
- 6) C. Lingner and B. Lüthi, *Phys. Rev. B* **23**, 256 (1981).
- 7) R. Camley and P. Fulde, *Phys. Rev. B* **23**, 2614 (1981).
- 8) R. Camley and P. Fulde, *Phys. Rev. B* **30**, 4137 (1984).
- 9) A. Wixforth, J. P. Kotthaus, and G. Weimann, *Phys. Rev. Lett.* **56**, 2104 (1986).
- 10) R. L. Willett, M. A. Paalanen, R. R. Ruel, K. W. West, L. N. Pfeiffer, and D. J. Bishop, *Phys. Rev. Lett.* **65**, 112 (1990).
- 11) P. Thalmeier, *Phys. Rev. B* **83**, 125314 (2011).
- 12) P. Thalmeier, B. Dóra, and K. Ziegler, *Phys. Rev. B* **81**, 041409(R) (2010).
- 13) T. Goto, H. Yamada-Kaneta, Y. Saito, Y. Nemoto, K. Sato, K. Kakimoto, and S. Nakamura, *J. Phys. Soc. Jpn.* **75**, 044602 (2006).
- 14) S. Baba, T. Goto, Y. Nagai, M. Akatsu, H. Watanabe, K. Mitsumoto, T. Ogawa, Y. Nemoto, and H. Yamada-Kaneta, *J. Phys. Soc. Jpn.* **80**, 094601 (2011).
- 15) S. Baba, M. Akatsu, K. Mitsumoto, S. Komatsu, K. Horie, Y. Nemoto, H. Yamada-Kaneta, and T. Goto, *J. Phys. Soc. Jpn.* **82**, 084604 (2013).
- 16) K. Okabe, M. Akatsu, S. Baba, K. Mitsumoto, Y. Nemoto, H. Yamada-Kaneta, T. Goto, H. Saito, K. Kashima, and Y. Saito, *J. Phys. Soc. Jpn.* **82**, 124604 (2013).
- 17) T. Goto, S. Sakatsume, A. Sawada, H. Matsui, R. Settai, S. Nakamura, Y. Ohtani, H. Goto, Y. Ohe, A. Tamaki, Y. Fuda, K. Abe, Y. Yamato, and T. Fujimura, *Cryogenics* **32**, 902 (1992).
- 18) O. V. Lounasmaa, *Experimental Principles and Methods Below 1K* (Academic Press, London, 1974) Chap. 6, p. 103.
- 19) R. C. Richardson and E. N. Smith, *Experimental Techniques in Condensed Matter Physics at Low Temperatures* (Addison-Wesley, Reading, MA, 1988) Chap. 2, p. 5.
- 20) R. Stoneley, *Proc. R. Soc. London, Ser. A* **232**, 447 (1955).
- 21) G. W. Farnell, in *Properties of Elastic Surface Waves, Physical Acoustics*, ed. W. P. Mason (Academic Press, New York, 2007) Vol. 6, Chap. 3, p. 109.
- 22) C. Kittel, *Introduction to Solid State Physics* (Wiley, New York, 2005) 8th ed., Chap. 3, p. 47.
- 23) T. C. Lim and G. W. Farnell, *J. Acoust. Soc. Am.* **45**, 845 (1969).
- 24) C. A. Coulson and M. J. Kearsley, *Proc. R. Soc. London, Ser. A* **241**, 433 (1957).
- 25) M. Lannoo, G. A. Baraff, and M. Schlüter, *Phys. Rev. B* **24**, 955 (1981).
- 26) G. A. Baraff and M. Schlüter, *Phys. Rev. Lett.* **41**, 892 (1978).
- 27) T. Yamada, Y. Yamakawa, and Y. Ōno, *J. Phys. Soc. Jpn.* **78**, 054702 (2009).
- 28) T. Ogawa, K. Tsuruta, and H. Iyetomi, *Solid State Commun.* **151**, 1605 (2011).
- 29) H. Matsuura and K. Miyake, *J. Phys. Soc. Jpn.* **77**, 043601 (2008).
- 30) R. Shiina, H. Shiba, and P. Thalmeier, *J. Phys. Soc. Jpn.* **66**, 1741 (1997).
- 31) S. Nakamura, T. Goto, S. Kunii, K. Iwashita, and A. Tamaki, *J. Phys. Soc. Jpn.* **63**, 623 (1994).
- 32) B. Lüthi, S. Blumenröder, B. Hillebrands, E. Zirngiebl, G. Güntherodt, and K. Winzer, *Z. Phys. B* **58**, 31 (1984).
- 33) Y. Nemoto, T. Yamaguchi, T. Horino, M. Akatsu, T. Yanagisawa, T. Goto, O. Suzuki, A. Dönni, and T. Komatsubara, *Phys. Rev. B* **68**, 184109 (2003).
- 34) S. Nakamura, T. Goto, M. Kasaya, and S. Kunii, *J. Phys. Soc. Jpn.* **60**, 4311 (1991).
- 35) V. Dohm and P. Fulde, *Z. Phys. B* **21**, 369 (1975).
- 36) B. Lüthi, *Physical Acoustics in the Solid State* (Springer, Heidelberg, 2005) Chap. 5, p. 67.
- 37) J. J. Sakurai, *Modern Quantum Mechanics* (Addison-Wesley, Reading, MA, 1985) 2nd ed., Chap. 3, p. 157.
- 38) S. M. Sze, *Semiconductor Devices* (Wiley, Hoboken, NJ, 2002) Chap. 6, p. 169.
- 39) The International Technology Roadmap for Semiconductors (ITRS), 2011 edition [<http://www.itrs.net>].